

Distributive Surface Load Position Estimation by Smart Optical Sensing

Lucas Hermann Negri*, Yujuan Wang*, Aleksander Sade Paterno†, Marcia Muller* and José Luís Fabris*

*Graduate School of Electrical Engineering and Computer Science
Federal University of Technology, Paraná, Brazil

E-mail: fabris@utfpr.edu.br, Telephone: +55 41 3310 4642

†Department of Electrical Engineering
Santa Catarina State University, 89223-100 Joinville, Brazil
E-mail: dee2asp@joinville.udesc.br

Abstract—This work proposes the usage of fiber Bragg gratings and artificial neural networks for distributive tactile sensing. Four fiber Bragg gratings were mounted on a polymethyl methacrylate rectangular plate. An artificial neural network was trained with experimental data to estimate the position of a cylindrical load on the plate. Results have shown a mean error corresponding to 1.37% of the sensing region's diagonal dimension. The obtained error is smaller than those achieved in literature, using a smaller number of sensors and a more compact neural network.

I. INTRODUCTION

A common strategy in the development of tactile sensing systems resides in point-to-point or array methods, where a number of point transducers are employed to monitor discrete positions [1], [2]. While this strategy is capable of fine-form discrimination, it is also costly for applications on extended surfaces due to the required number of sensors. Also, it is desirable that the response of each individual sensor to be restricted to its local area, with a low cross-coupling between neighbor sensors.

Another way to develop tactile systems is by using distributive sensing. The distributive tactile sensing method employs a continuous mechanical element, such as an elastic surface that deforms in the presence of a load. This deformation is sensed by a reduced number of sensors placed on different points of the surface, and the outputs of the sensors are then combined to estimate properties of the applied load. Distributive tactile sensing has been applied for the detection of the shape and position of loads in 1D and 2D systems [3], to determine the deformation on a plate [4], and to track the position of a moving load along a plate [5]. Artificial neural networks (ANN) can be employed to learn an approximate relation between sensor outputs and load properties, such as the position and shape of the load [3] or its movement [5]. Recently, it was shown the usage of fiber Bragg optical sensors and ANNs in the localization of surface impacts [6].

This preliminary work proposes the usage of fiber Bragg gratings (FBG) with artificial neural networks for the distributive sensing of the position of a cylindrical load on a rectangular plate. In this context, the use of FBGs is interesting mainly due to its intrinsic strain sensitivity, multiplexing capabilities,

small size, passivity (absence of electrical components on the transducer) and no influence on the plate elasticity. Artificial neural networks are employed here to determine the relation between the FBGs' output and the load position by using experimental data instead of an analytic solution. Experimental results are shown and compared to similar works.

II. METHODOLOGY

A. FBG Strain Sensing

A simple FBG consists in the periodic modulation of the core's refractive index of a single mode optical fiber [7]. This modulation results in the reflection of the incident light with wavelength close to the grating resonance wavelength λ_b , given by Equation 1:

$$\lambda_b = 2n_{eff}\Lambda, \quad (1)$$

where n_{eff} is the effective refractive index of the core and Λ is the grating's pitch. Straining the FBG or changing its temperature results in changes to both Λ and n_{eff} [7], thus changing λ_b . More specifically, the strain ϵ will result in a wavelength shift given by Equation 2 [7]:

$$\Delta\lambda_b = \lambda_b(1 - p_e)\epsilon, \quad (2)$$

where p_e is the strain-optic constant given by Equation 3:

$$p_e = \frac{n_{eff}^2}{2} [p_{12} - \nu(p_{11} + p_{12})]. \quad (3)$$

Typical values for the strain-optic tensor components and the Poisson ratio are $p_{11} = 0.113$, $p_{12} = 0.252$, and $\nu = 0.16$ [8]. By assuming an effective refractive index of 1.482 and an original λ_b of 1535 nm, a strain of $82.737\mu\epsilon$ is required for a $\Delta\lambda_b$ equal to 100 pm. Besides being sensitive to strain, an FBG is also sensitive to temperature. The wavelength shift $\Delta\lambda_b$ caused by the temperature variation ΔT is given by Equation 4 [7]:

$$\Delta\lambda_b = \lambda_b(\alpha_\Lambda + \alpha_n)\Delta T, \quad (4)$$

The authors would like to thank the financial support received from CAPES, CNPq, FINEP, and Fundação Araucária (Brazilian Agencies).

where α_Λ is the thermal expansion coefficient and α_n is the fiber thermo-optical coefficient, with typical values of 0.55×10^{-6} and 8.6×10^{-6} , respectively [7]. For an original λ_b of 1535 nm, a ΔT of 7.12 K is required for a $\Delta\lambda_b$ of 100 pm. The use of an FBG as a strain sensor usually requires temperature control or the usage of a reference FBG to compensate for temperature effects.

B. Experimental Setup

A rectangular sensing surface (31.8 cm \times 30.7 cm) was developed by using a polymethyl methacrylate (PMMA) plate, 0.5 cm thick. The plate is supported by four silicone hemispheres placed at its four corners, as shown in Figure 1. The hemispheres present a radius of 0.3 cm, and were glued to the plate. This positioning permits the plate to deform under transverse forces.

Four FBGs were placed at the plate's underside in order to sense plate deformations. The FBGs were spliced into a single fiber and positioned on the two diagonals of the plate, as depicted in Figure 1. This diagonal disposition was implemented to maximize the response of the FBGs [9]. Each FBG was initially positioned by using adhesive tape and subjected to a previous strain, and then properly held to the plate by using cyanoacrylate adhesive. A linear graph paper sheet, with millimeter graduation, was placed on top of the plate to help the load positioning.

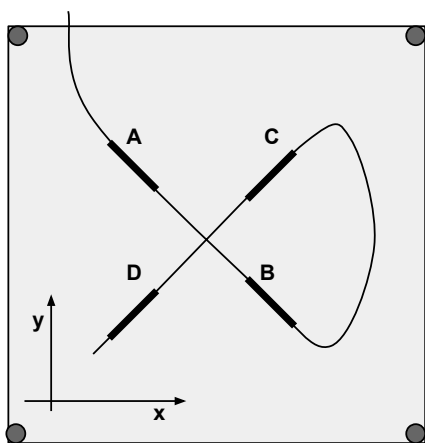


Fig. 1. Schematic diagram (top view) showing the four FBG sensors (A, B, C, D).

The employed FBGs present different resonance wavelengths to allow the interrogation by frequency multiplexing. Specifically, the resonance wavelengths of the FBGs shown in Figure 1 are: A = 1539.402 nm, B = 1535.304 nm, C = 1530.964 nm and D = 1527.288 nm at 23 °C, measured before the mounting on the plate and the pre-straining. A broadband light emitting diode (Superlum PILOT 2 LED, centered at 1558.2 nm with a FWHM of 73.8 nm), was used to interrogate the FBGs. The light reflected by FBGs is collected by an optical interrogator (Ibsen I-MON E512, resolution < 0.5 pm) at an interrogation rate of approximately 20 spectra per second. This optical setup is shown in Figure 2. The peak wavelengths of the reflected spectrum were computed by using Gaussian fitting. The experiments were performed in

an air-conditioned room, with the temperature control set to 23 °C.

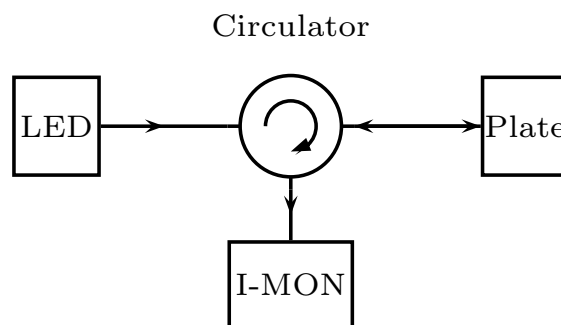


Fig. 2. Experimental setup: the LED illuminates the FBGs on the plate, whose reflected light spectra is analyzed by using the I-MON unit.

A cylindrical load, with mass of 0.5 kg and radius of 1 cm was used in the experiments. The load was placed (centered) on distinct points of the surface, comprised in a 20 cm \times 20 cm restricted area centered on the plate, in order to avoid regions close to the edges. Two spectra were recorded for each load, one before as reference and one after the placement. The reference spectrum was used to compensate for thermal variations and mechanical creep. To further reduce the undesirable fluctuating effects on the mechanical creep, spectra were recorded at least 5 s after removing or placing the load on the sensing surface.

Placements were performed on a symmetrical grid with points separated by steps of 5 cm, on both axes, totaling 25 points. These 25 placements were repeated 3 times, resulting in 3 data sets.

C. Load Position Estimation

An artificial neural network was employed to estimate the load position on the sensing surface. The ANN presents a multilayer perceptron topology, with four neurons in the input layer, five neurons in the singleton hidden layer and two neurons in the output layer. The inputs to the ANN are the peak wavelength shifts (before and after loading) of the four FBGs, and the outputs are the estimated position of the load on the x and y axes. All neurons employed a symmetric sigmoidal activation function, with all the inputs and outputs linearly scaled to the -1 to 1 range in order to match the activation function's operating range.

The training of the ANN was achieved by using the Neuron-by-Neuron algorithm [10] and random initial synaptic weights. The ANN was trained with one of the three data sets. The network topology and parameters were chosen so that the error for a second data set (validation data set) was minimized. Lastly, the developed ANN was tested with the third unseen data set to estimate the network's generalization capabilities.

Three different error metrics were established: the mean Euclidean distance (error) between the actual point and the estimated point, the mean absolute error on the x axis, and the mean absolute error on the y axis.

III. RESULTS AND DISCUSSION

The obtained experimental results are shown in Table I. One should notice that the Euclidean error can not be computed from the final mean absolute error on the axes.

TABLE I. EXPERIMENTAL RESULTS FOR THE THREE ERROR METRICS.

Metric	Value [cm]
Mean absolute error on the x axis	0.273
Mean absolute error on the y axis	0.165
Euclidean error	0.388

The measured strain responses of the four mounted FBGs are shown in Table II, representing the maximum and mean wavelength shifts during the acquisition of the test data set.

TABLE II. STRAIN RESPONSES OF THE EMPLOYED FBGs DURING THE EXPERIMENTS.

FBG	Max. $\Delta\lambda_b$ [pm]	Mean $\Delta\lambda_b$ [pm]
A	111	37
B	128	53
C	118	38
D	142	50

Figure 3 shows an Euclidean error map, computed with the test data. This map was built by interpolating the Euclidean errors to improve its visualization.

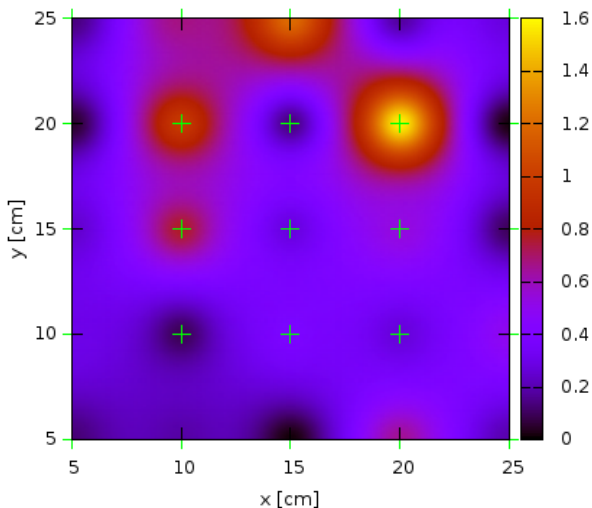


Fig. 3. Error map built by interpolating the Euclidean error, in cm, computed with the test data. The crosses represents the actual points of the test data.

The cylindrical load was placed and removed repeatedly at point $x = 15$ cm and $y = 15$ cm, with the corresponding wavelength shifts (FBG B) shown in Figure 4. A more detailed view of the wavelength shifts caused only by the mechanical creep and temperature variations is seen in Figure 5, which corresponds to the shifts (FBG B) shortly after the placement and removal of the load.

The Euclidean error shown in Table I corresponds to 1.37% of the restricted placement area's diagonal. The corresponding root mean square error is equal to 1.93% of the diagonal,

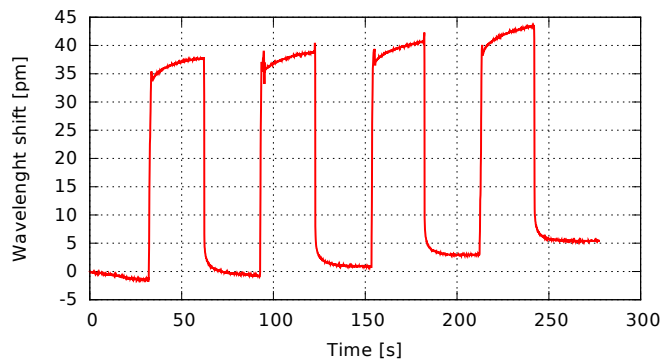


Fig. 4. Wavelength shifts (FBG B) after a sequence of placements and removals of the the cylindrical load at position $x = 15$ cm and $y = 15$ cm.

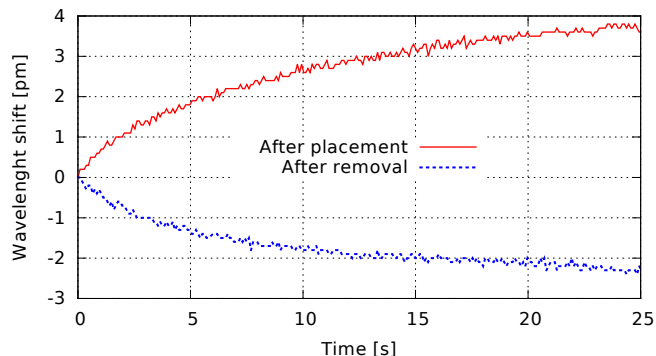


Fig. 5. Wavelength shifts (FBG B) due to mechanical creep and temperature changes after one placement and one removal of the cylindrical load at the point $x = 15$ cm and $y = 15$ cm.

which is smaller than the 2.7% error reported by Cowie et al [3]. Also, it should be noticed that this work proposes a simpler approach than described by Cowie et al [3], by using 4 FBGs instead of 9 and a more compact ANN with 5 hidden neurons instead of 42, albeit using a smaller sensing area.

As shown in Table II, the FBGs present different strain responses, despite having approximately the same structure and sensitivities. This result indicates that the FBGs are not symmetrically positioned, and that the pre-tensioning was not uniform among the four gratings. The difference between the error on the x and y axes can also be a result of this asymmetrical positioning.

When observing the approximate error map shown in Figure 3, one can see that there are some points where the Euclidean error is distinctly higher than the others. These errors may have been caused by the mechanical creep evidenced in Figure 4.

The variations shown in Figures 4 and 5 can be explained by two factors: temperature variations on the FBGs, and the plate's mechanical creep. Those error factors can be attenuated by reading a reference spectrum before each position estimation, as performed in this work. Nevertheless, it can be a limiting factor. To overcome this drawback, one could place an unstrained FBG on the sensing region to compensate temperature variations. Other materials and methods to fixate the FBGs could be tried in order to minimize the mechanical

creep, which is assumed to be the greatest contributor to the estimation error. Also, the sensor locations could be optimized to enhance the estimation performance, as already proposed in literature [11], [12].

IV. CONCLUSION

This work proposed the usage of FBGs and a distributive manner to estimate the position of a cylindrical load on a PMMA plate. Experiments showed superior results than those already reported in literature [3] while using a simpler approach with a reduced number of FBGs and a more compact ANN. Albeit attenuated by using a reference reading, the mechanical creep, temperature variations, and permanent changes in the pre-tensioning of the FBGs were identified as primary error sources. Future works include the reduction of error sources by experimenting different methods to fixate the FBGs on the plate, different plate materials, the development of a methodology capable of estimating the position for different load weights, and the optimization of the sensors' positions.

REFERENCES

- [1] A. Caiti, G. Canepa, D. De Rossi, F. Germagnoli, G. Magenes, and T. Parisini, "Towards the realization of an artificial tactile system: fine-form discrimination by a tensorial tactile sensor array and neural inversion algorithms," *IEEE Trans. Syst. Man. Cybern.*, vol. 25, no. 6, pp. 933–946, Jun. 1995.
- [2] J.-S. Heo, K.-Y. Kim, and J.-J. Lee, "Development of a Distributed Force Detectable Artificial Skin Using Microbending Optical Fiber Sensors," *J. Intell. Mater. Syst. Struct.*, vol. 20, no. 17, pp. 2029–2036, Sep. 2009.
- [3] B. M. Cowie, D. J. Webb, B. Tam, P. Slack, and P. N. Brett, "Fibre Bragg grating sensors for distributive tactile sensing," *Meas. Sci. Technol.*, vol. 18, no. 1, pp. 138–146, Jan. 2007.
- [4] Y. Wang, N. Chen, B. Yun, and Y. Cui, "Use of Fiber Bragg Grating Sensors for Determination of a Simply Supported Rectangular Plane Plate Deformation," *IEEE Photonics Technol. Lett.*, vol. 19, no. 16, pp. 1242–1244, Aug. 2007.
- [5] M. Elliott, X. Ma, and P. Brett, "Tracking the position of an unknown moving load along a plate using the distributive sensing method," *Sensors Actuators A Phys.*, vol. 138, no. 1, pp. 28–36, Jul. 2007.
- [6] F. Ribeiro, G. R. C. Possetti, J. L. Fabris, and M. Muller, "Smart optical fiber sensor for impact localization on planar structures," in *Microwave & Optoelectronics Conference (IMOC), 2013 SBMO/IEEE MTT-S International*. IEEE, 2013, pp. 1–3.
- [7] A. Othonos and K. Kalli, *Fiber Bragg gratings: fundamentals and applications in telecommunications and sensing*. Artech House, 1999.
- [8] A. Bertholds and R. Dandliker, "Determination of the individual strain-optic coefficients in single-mode optical fibres," *J. Light. Technol.*, vol. 6, pp. 17–20, 1988.
- [9] F. Ribeiro, "Sensor inteligente em fibra ótica para localização de deformações em estruturas planas," Master's thesis, Universidade Tecnológica Federal do Paraná, 2014.
- [10] B. Wilamowski, "Neural network architectures and learning algorithms," *IEEE Ind. Electron. Mag.*, vol. 3, no. 4, pp. 56–63, Dec. 2009.
- [11] S. Rapp, L.-H. Kang, J.-H. Han, U. C. Mueller, and H. Baier, "Displacement field estimation for a two-dimensional structure using fiber Bragg grating sensors," *Smart Mater. Struct.*, vol. 18, no. 2, p. 025006, Feb. 2009.
- [12] R. T. Jones, D. G. Bellemore, T. A. Berkoff, J. S. Sirkis, M. A. Davis, M. A. Putnam, E. J. Friebele, and A. D. Kersey, "Determination of cantilever plate shapes using wavelength division multiplexed fiber Bragg grating sensors and a least-squares strain-fitting algorithm," *Smart Mater. Struct.*, vol. 7, no. 2, pp. 178–188, Apr. 1998.